Article submitted to: High Power Laser Science and Engineering, 2025 *September 16, 2025*

High-Power Near-Single-Mode Fiber Laser Based on the Low-NA Confined-Doped Fiber: Numerical Investigation and 6.74 kW Experimental Validation

Cheng Yang[1,†], Haobo Li[1,†], Pengcheng Geng[3], Hanshuo Wu[1,2], Yize Shen[3], Xin Yi Ding[1], Xiaoming Xi[1,2], Zhiping Yan[1,2], Chunxiao Zhao[1,2], Suyu Wang[3], Liangjin Huang[1,2], Zhiyong Pan[1,2], Xiaolin Wang[1,2], Yongqing Yi[3], and Pu Zhou[1]

[1]*College of Advanced Interdisciplinary Studies, National University of Defense Technology, Changsha 410073, China*
[2]*Nanhu Laser Laboratory, National University of Defense Technology, Changsha 410073, China*
[3]*Tianjin Key Laboratory of Special Optical Fiber Materials, Tianjin 300220, China*
[†]*These authors contributed equally*

Abstract
In this study, we present a low numerical aperture (NA) confined-doped fiber architecture that synergistically mitigates transverse mode instability (TMI) through combined optical waveguide engineering and spatially tailored gain distribution. The individual and combined benefits of low NA fiber design and the confined-doped fiber design strategy on TMI mitigation are numerically investigated. Building upon these theoretical analyses, a self-developed fiber, featuring a core/cladding diameter of ∼26/400 μm, core NA of ∼0.045, core doping ratio of ∼75%, is fabricated. Further experimental validation in a master oscillator power amplifier demonstrates 6.74 kW output power with near-single-mode (M^2∼1.49) beam quality, validating the design's efficacy. This study establishes a novel fiber design paradigm that concurrently addresses TMI mitigation, beam quality maintenance, and power scalability, offering a viable pathway toward robust high-power fiber laser sources with near-diffraction-limited beam quality.

Keywords: confined-doped fiber; low numerical aperture fiber; high power; near single-mode beam quality; bidirectional pump

1. Introduction

Fiber lasers are extensively employed in diverse fields, including industrial processing, energy exploration, medical treatment, and scientific research [1-4]. These applications typically demand high power and excellent beam quality. However, power scaling in ytterbium-doped fiber lasers is primarily constrained by nonlinear effects and transverse mode instability (TMI) [5, 6]. In recent years, the conventional large-mode-area (LMA) fibers with a step-index profile have been widely used as a gain medium in high-power fiber lasers to reduce the influence of nonlinear effects, especially the stimulated Raman scattering (SRS), and achieve high-power output laser [7]. However, the LMA fibers with a larger core diameter can support more high-order modes (HOMs), which would result in beam quality degradation and a lower TMI threshold. Therefore, it is difficult to simultaneously achieve high power and good beam quality. To balance the SRS suppression and TMI mitigation, various specialty optical fibers have been proposed, such as long tapered fibers [8-10], low numerical aperture (NA) fibers [11-13], large-pitch fibers [14-16], photonic crystal fibers [17-19] and confined-doped fibers [20-22], among which, the confined-doped fiber is easier to implement and has proven its capability in high-brightness fiber laser generation [23-29].

The confined-doped fiber is designed to provide preferential gain to the expected transverse modes by selective doping within the core, which is known as the gain filtering effect [30]. In the confined-doped fibers, usually the center of the core is doped, since the fundamental mode (LP_{01}) mainly occupies the central region of the core, it can extract more gain and thus dominate the output laser. In terms of near sin-

Correspondence to: H. Wu, X. Wang, P. Zhou. College of Advanced Interdisciplinary Studies, National University of Defense Technology, Changsha 410073, China Email: whsopt@126.com (H. Wu); Email: chinaphotonics@163.com (X. Wang);Email: zhoupu203@163.com (P. Zhou)

10.1017/hpl.2025.10070
https://doi.org/10.1017/hpl.2025.10070 Published online by Cambridge University Press

gle mode operation (beam quality factor $M^2 < 1.5$), in 2016, Mashiko et al. from Fujikura reported a 2 kW bidirectional pump confined-doped oscillator with beam quality factor M^2 ~1.2 [23]. By optimizing the pump power allocation, the output power was further improved to 3 kW with M^2 ~1.3 [24], proving the great potential of the confined-doped in power scaling and beam quality maintaining. In 2022, Zhang et al. demonstrated a bidirectional pumped all-fiber amplifier, of which a 4.18-kW single-mode (M^2 ~1.3) laser output is achieved by employing a low NA confined-doped long-tapered Yb-doped fiber [31]. As for confined-doped fiber lasers with higher output power, the tandem pumping scheme are mostly employed and the beam qualities deviate from near single mode. In 2018, Seah et al. built a tandem-pumped fiber amplifier using confined-doped fiber with 4.1 kW output power and M^2 ~1.59, which was much better than its full-doped fiber amplifier counterpart [25]. In 2022, Wu et al. fabricated a confined-doped fiber with the core/cladding diameter of 40/250 μm and doping ratio of ~75%. Based on a bidirectional tandem-pumped amplifier, 7.88 kW output power was realized with the beam quality factor of M^2 ~1.97 [32]. Later that year, they improved the output power to over 10 kW with the M^2 ~2.16 [22], which is the highest power of confined-doped fiber laser ever reported.

Based on the above-mentioned experimental results, it can be recognized that achieving higher output power while maintaining near-single-mode beam quality in confined-doped fibers presents a significant challenge. Examining the operation mechanism of confined-doped fibers, it is evident that these fibers are designed to confer preferential gain to specific transverse modes, rather than incurring preferential loss across different modes, indicating the inevitably generated HOMs at fiber splicing point would experience power amplification in the confined-doped fiber. Therefore, the proportion of the HOMs in the output laser is largely determined by the doping ratio. In the above-mentioned fiber lasers, the doping ratio is larger than the optimum value (typically ~0.5) in order to guarantee sufficient pump absorption with a short fiber length. Therefore, the HOMs would extract considerable gain and degrade the beam quality, making it extremely hard to realize near-single-mode laser operation. While reducing the doping ratio can suppress the amplification of HOMs, this approach inherently compromises pump absorption efficiency. Balancing beam quality maintenance, pump efficiency, and power scalability therefore represents a critical challenge in high-power fiber laser design.

To address this challenge, a promising strategy involves introducing discriminative loss mechanisms specifically targeting HOMs. A direct and practical approach to achieve this is through the incorporation of a low NA fiber design. By reducing mode confinement, such a configuration enhances bending-induced loss for HOMs even at relatively large bending diameters, effectively suppressing their amplification without inducing significant perturbations to the fundamental mode. This approach leverages the inherent sensitivity of HOMs to geometric perturbations. The feasibility, implementation methodology, and performance efficacy of this design warrant systematic investigation to validate its potential for scalable high-power fiber laser systems.

In this study, we proposed the fiber design simultaneously integrating the low optical confinement (low-NA design) and spatially tailored gain distribution (confined-doping design), where the theoretical analysis was carried out to distinguish the benefits of low-NA design and confined-doped design for TMI mitigation, and consequently a low-NA confined-doped fiber with a core/cladding diameter of 26/400 μm is successfully fabricated, with Yb-ions doping diameter ratio of ~75%, and core NA of 0.045. As a result, a 6.74 kW output power with the beam quality M^2 factor~1.49 is demonstrated based on the self-developed specialty fiber in a bidirectional laser diode (LD) pump scheme.

2. Theoretical Analysis

Previous study shows that confined-doped fibers with a relative doping ratio of less than 0.6 have the potential to achieve single-mode fiber laser output, which, however, requires excessively long fiber lengths for sufficient pump absorption, and the power scaling would be limited by the SRS effect [21]. Increasing the relative doping ratio would increase the overlap between higher-order modes and the doped region, which weakens the gain-filtering effect, leading not only to beam quality degradation but also to a reduction in the TMI threshold. To balance the mitigation of SRS effect and the TMI effect in confined-doped fiber with doping ratio being larger than the optimum value, we integrate the low-NA design into the confined-doped fibers as an alternative to the conventional low-doping-ratio gain fibers to facilitate near-single-mode operation. To assess the feasibility of the proposed scheme, the TMI thresholds of the two types of fibers are theoretically investigated. We use a TMI theoretical model based on coupled-beam theory to calculate the TMI threshold of the confined-doped fiber amplifier, where the mode coupling equations for the LP_{01} mode and LP_{11} mode can be expressed as:

$$\frac{dP_1}{dz} = (g_1 - \alpha_1) P_1 - g_1 \chi P_2 P_1 \tag{1}$$

$$\frac{dP_2}{dz} = (g_2 - \alpha_2) P_2 + g_1 \chi P_1 P_2 \tag{2}$$

where, subscripts 1 and 2 represent the LP_{01} mode and LP_{11} mode, respectively. *P* denotes the signal power, *g* represents the pump gain, α is the mode loss, and χ is the nonlinear coupling coefficient, derived from reference[24]. The power

https://doi.org/10.1017/hpl.2025.10070 Published online by Cambridge University Press

of the LP_{11} mode can be expressed as:

$$P_2(z) = P_2(0)\exp\left[\int_0^z \left(g_2(z') - \alpha_2(z') + g_1(z')\chi(z')P_1(z')\right)dz'\right] \quad (3)$$

where, $P_2(0)$ is the initial power of the LP_{11} mode. The output power at which the power of the LP_{11} mode reaches 1% of the total power at any position along the fiber is defined as the TMI threshold. A forward pump fiber amplifier is assumed in the simulation, where the core/cladding diameter of the gain fiber is set to 26/400 μm, the pump wavelength is 976 nm, and the signal wavelength is 1064 nm. The Yb-doping concentration is 5×10^{25} m^{-3}, the seed power is 30 W, and the bending diameter ($2R_b$) is set to 30 cm to alleviate the bend-induced mode distortion.

According to the above theoretical model, the TMI threshold and the overlap integral between the transverse mode and the doped region (the energy proportion of transverse modes in the doped region) are calculated and illustrated in Figure 1(a). First, the overlap integral in both the bent and unbent states is very close, indicating that the bend-induced mode distortion is negligible. Therefore, the subsequent simulation results do not take into account the effects of bending distortion. When the core NA is 0.06, as the relative doping ratio increases from 0.6 to 0.75, the overlap integral of the LP_{11} mode with the doped region increases from 0.33 to 0.58, as shown in Figure 1(a), leading to a decrease in the TMI threshold from 8000 W to 4439 W, as shown in Figure1(b). Upon reducing the core NA to 0.045, the LP_{11} mode exhibits increased lateral spread owing to the lower mode confinement, and the overlap integral of the LP_{11} mode with the doped region decreases from 0.58 to 0.45, and the TMI threshold of the confined-doped fiber amplifier with a relative doping ratio of 0.75 increases to 5114 W. It is noteworthy that in the above analysis, the HOM losses are disregarded, and the assessment is focused solely on the impact of the overlap factor change induced by the NA change. The results indicate that the low-NA design can reduce the overlap factor between the LP_{11} mode and the doping region, therefore making it less demanding on the doping diameter.

Further considering the additional increment in bending loss (2.1 dB/m for LP_{11} mode, neglectable bending loss for LP_{01} mode) attributed to the diminished NA of 0.045, the TMI threshold is ultimately elevated to 7524 W, as shown in Figure 1(b). The TMI threshold of confined-doped fibers with a core NA of ~0.045 and a relative doping ratio of 0.75 is comparable to that of confined-doped fiber with a core NA of ~0.06 and a relative doping ratio of 0.6. Therefore, the high bending loss for HOMs brought by the low-NA design can also contribute to TMI mitigation.

Moreover, to distinguish the TMI mitigation effect of gain filtering from the bending loss in this fiber, the TMI thresholds of the fiber amplifier employing the conventional fully-doped fiber with the same core and cladding diameter are calculated. As shown in Figure 1(b), fiber amplifier based on the conventional fiber with core NA of 0.045 has the TMI threshold of 2307 W, which is only ~31% of the amplifier employing confined-doped fiber with doping ratio of 0.75, indicating the gain filtering effect brought by confined-doping design also play a significant role in TMI mitigation.

Therefore, by reducing the core NA, the confined-doped fiber with a relatively high doping ratio can achieve comparable performance to confined-doped fiber with optimum doping ratio (usually a low doping ratio ~0.6), which brings new insights into the design of high performance confined-doped fiber for near-single-mode laser operation.

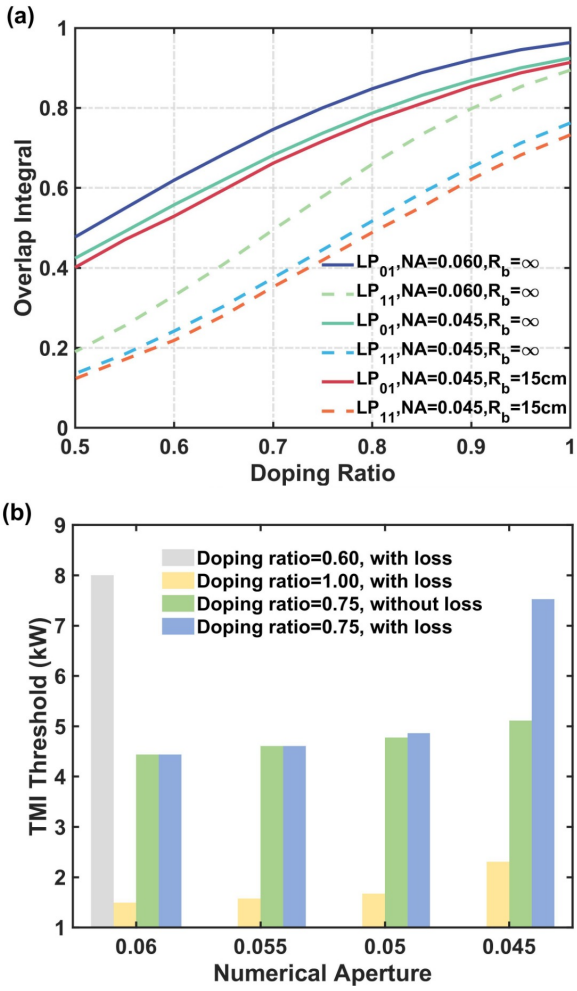

Figure 1. The impact of NA and relative doping ratio on the (a) overlap integral of LP_{01} mode (solid line) and LP_{11} mode (dashed line) and (b) TMI threshold.

https://doi.org/10.1017/hpl.2025.10070 Published online by Cambridge University Press

3. Fiber characterization and experimental setup

Based on the theoretical investigation on the individual and combined effects of low NA and confined-doping on the TMI threshold, a low NA confined-doped fiber with a core/cladding diameter of 26/400 μm is designed and fabricated. The cross section of the developed fiber is shown in Figure 2, implying a core diameter of ∼25.88 μm and a cladding diameter of ∼406.36 μm. The confined-doped fiber preform rod is made based on Modified Chemical Vapor Deposition (MCVD) process combined with rare earth chelate compound gas-phase doping technology. The core layer of the fiber preform consists of 8 layers. The inner 5 layers composed of SiO_2, Yb_2O_3, P_2O_5, Al_2O_3, SiF_4. The composition of the outer three core layers is SiO_2, Al_2O_3, SiF_4. After the 8-layer core layer deposition is completed, the hollow preform needs to be collapsed into a solid preform through a high-temperature rod shrinking process. The weight percentage distribution of F, Al_2O_3, P_2O_3,Yb_2O_3 of the confined-doped fiber (derived from electron probe micro analyzer) is shown in Figure 3. Figure 4 shows the refractive index profiles at two positions (A and B) along the fiber, spaced approximately 20 meters apart, as well as the weight percentage distribution of Yb_2O_3 in the confined-doped fiber. The refractive index distributions at these two positions are quite similar, and the fluctuation of the radial refractive index distribution of the fiber is reduced compared with the fiber preform. The core diameter is ∼25.88 μm and the Yb-ions doping diameter is ∼19.49 μm, indicating a relative doping ratio of ∼75.31%. The core NA is approximated to be ∼0.045 according to the refractive index profile. However, during the high-temperature rod shrinking process, when the heating temperature reaches above 2200°C, elements such as ytterbium, fluorine, and phosphorus in the central core layer will evaporate due to heat, while other core layers are far away from the surface, and elements such as ytterbium, fluorine, and phosphorus will not evaporate. The above reasons will result in a more obvious central dip of the refractive index distribution profile and ytterbium concentration distribution profile, as shown in Figure 4. The pump absorption is measured to be ∼1 dB/m@976 nm through the cutback method. The attenuation loss of the confined-doped fiber is measured to be ∼13.5 dB/km@1200 nm.

The experimental setup of the bidirectional LD pumped confined-doped fiber amplifier is shown in Figure 5. The seed laser is a 100 W-level fiber laser operating at 1080 nm. To remove the residual pump light from the backward pump, a cladding power stripper (CPS) is adopted before the amplifier stage. The pump sources are based on 976 nm wavelength-stabilized LDs. Four 400 W-level LDs and eleven 250 W-level LDs serve as forward pump sources, while fifteen 400 W-level LDs serve as backward pump sources. All the LDs are injected into the fiber amplifier through the forward and backward (18+1)×1 power and

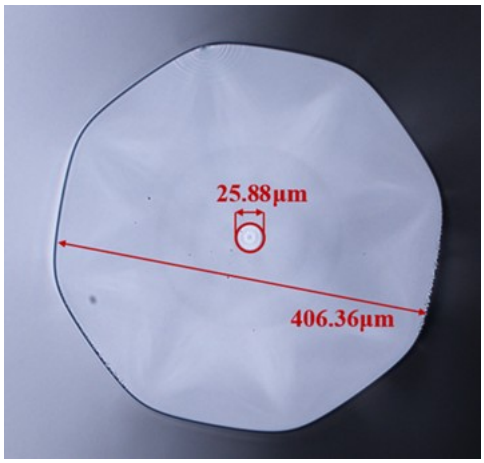

Figure 2. The cross section of the developed fiber.

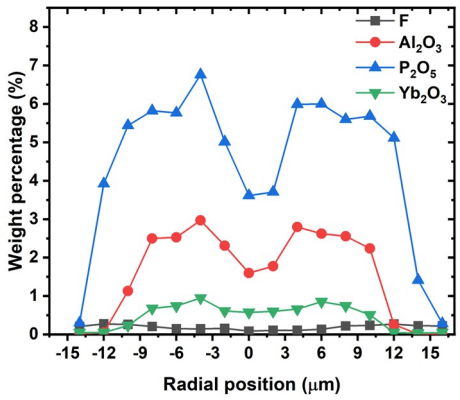

Figure 3. Weight percentage distribution of F, Al_2O_3, P_2O_3,Yb_2O_3 of the confined-doped fiber.

signal combiners (PSCs), which consists of 18 pump ports with a core/cladding diameter of 135/155 μm and a signal fiber with a core/cladding diameter of 30/250 μm. The YDF is 20 m in length and is spirally-coiled on a water-cool plate, and the temperature of the water cooling system is set to 20 °C, with temperature fluctuation less than ±1 °C. The seed laser and the forward pump power enters the fiber amplifier from the innermost circle while the backward pump power enters the fiber amplifier from outmost circle of the gain fiber. Although the core size of the 26/400 μm gain fiber is not optimally matched with that of the 30/400 μm combiner signal fiber, the splice loss between the two fibers is controlled to approximately 0.01 dB by rationally setting the splicing parameters. The amplified laser from the fiber amplifier passes through the CPS and outputs via the quartz block head (QBH). All the components are fixed on the water-cooled plates to achieve efficient thermal management. The experimental measurement setup comprises a power meter (PM), an optical spectrum analyzer

https://doi.org/10.1017/hpl.2025.10070 Published online by Cambridge University Press

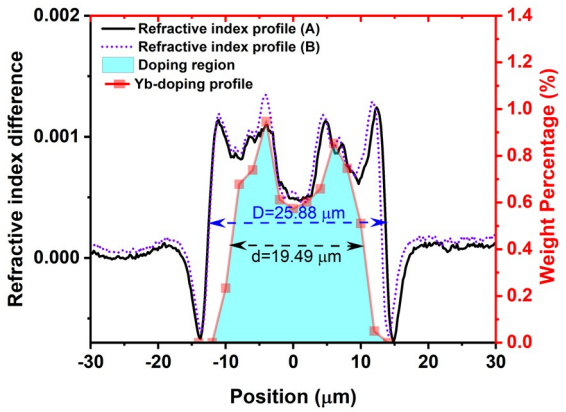

Figure 4. Refractive index profile and Yb_2O_3 weight percentage distribution of the confined-doped fiber.

(OSA), a beam quality analyzer (BQA), and an oscilloscope with a photodetector (PD), to measure the output power, spectra, and time domain simultaneously. The output laser is first collimated by the collimator and most of the power is reflected by the high reflection mirror (HR) and enters the PM for power measurement. The diffracted beam is monitored by the PD and OSA for time domain and spectrum measurement. The transmitted laser then passes through the optical filter (OF) to filter out the insignificant pump power, and then enters the BQA for beam quality measurement.

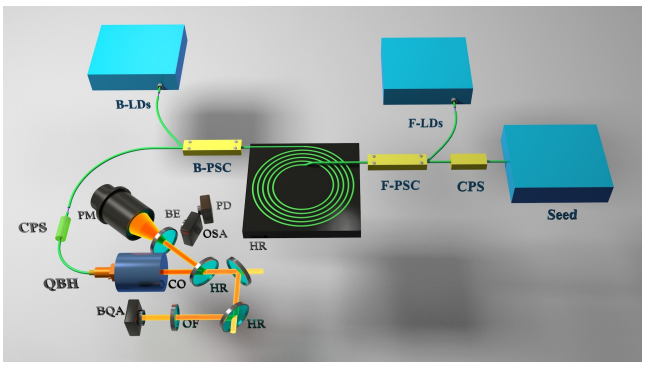

Figure 5. Experimental setup of the bidirectional pumped confined-doped fiber amplifier. (LD: laser diode, F-PSC: forward pump and signal combiner, B-PSC: backward pump and signal combiner, CPS: cladding power stripper, QBH: quartz block head, CO: collimator, HR: high reflection mirror, BE: beam expander, OSA: optical spectrum analyzer, OF: optical filter, BQA: beam quality analyzer, PD: photodetector, PM: power meter.)

4. Results and discussion

We first conducted a counter-pump experiment to investigate the TMI threshold under various bending diameters. The TMI thresholds with different inner bending diameters (referring to the bending diameter of the innermost circle) of self-developed YDF under the counter-pump scheme are summarized in Table 1, and the laser power as a function of pump power under different inner bending diameters is shown in Figure 6. When the inner bending diameter decreases from 44 cm to 26 cm, the TMI threshold exhibits an increasing trend, rising from 3820 W to 4580 W. This is attributed to the enhanced bending loss of higher-order modes (HOMs), which facilitates a higher TMI threshold. When the inner bending diameter is further decreased to 25 cm, the TMI threshold drops to 4260 W, which is owing to the greater fundamental mode loss at this bending diameter. This can be distinguished from the decreasing overall efficiency from more than 83% to less than 80% at the same pump power. Thus, this fiber amplifier with the inner bending diameter of 26 cm can achieve the highest TMI threshold and, therefore, bending diameter is fixed at 26 cm throughout the study for further investigation.

Table 1. The TMI threshold under different inner bending diameters

Inner Bending Diameter/cm	TMI Threshold/W
44	3820
30	4440
28	4510
26	4580
25	4260

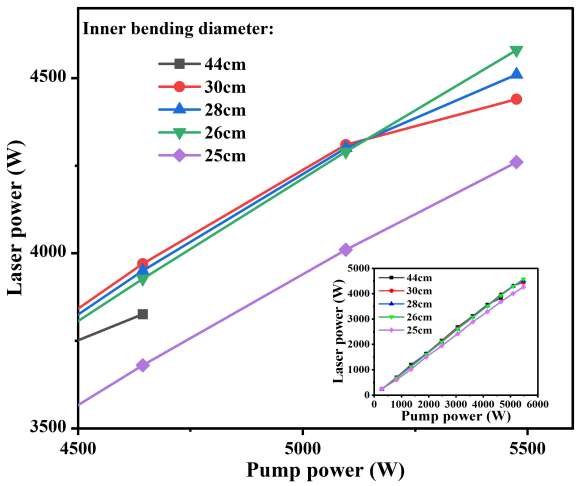

Figure 6. Laser power as a function of pump power under different inner bending diameter. Inset: output power within whole pump power range

The experimental results at the inner bending diameter of 26 cm are shown in Figure 7. The seed laser power was measured to be approximately 40 W after passing through the amplifier stage. As shown in Figure 7(a), the output power linearly increases with the pump power, with a slope efficiency of ~83.6%. When the pump power is 5475 W, the output power reaches 4580 W. There is no residual pump light and Stokes light components on the spectrum during

https://doi.org/10.1017/hpl.2025.10070 Published online by Cambridge University Press

the power scaling process, as shown in Figure 7(b). Further increasing the output power results in obvious fluctuations in the time-domain signal, and typical TMI characteristic frequencies are observed in its corresponding Fast Fourier Transform (FFT) results, as shown in Figure 7(c). The M^2 factor is measured and recorded throughout the experiment. The M^2 factor as a function of output power is shown in Figure 7(d). When the output power increases from 40 W to 4580 W, the M^2 factor slightly increases from 1.34 to 1.39, maintaining a near-single-mode beam quality.

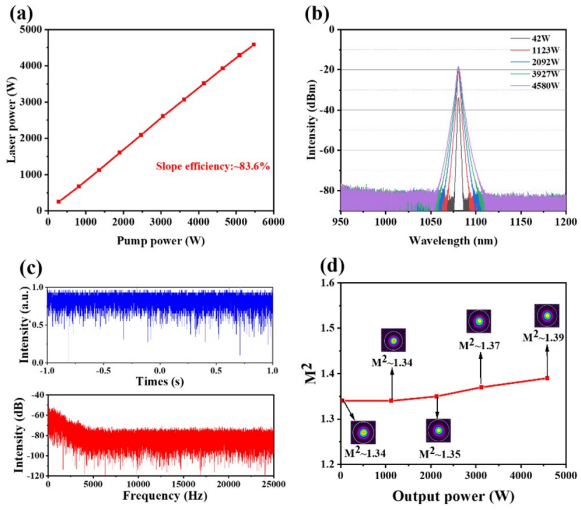

Figure 7. (a) Output power as a function of pump power in counter-pump scheme; (b) Output spectra under different output power in counter-pump scheme; (c) Time-domain signal and the corresponding FFT spectrum at 4580 W; (d) M^2 factor as a function of output power in counter-pump scheme. Insert: beam profiles at different output power.

Therefore, the power scaling of this amplifier under the condition of counter-pump is limited by TMI, and the threshold is about 4580 W. Then, a co-pump experiment is conducted using three groups of 976 nm LDs, which can provide more than 4 kW pump power. The inner bending diameter of YDF remains at 26 cm, which has the highest TMI threshold under counter-pump. The experimental results are shown in Figure 8. The seed laser power remained at approximately 40 W. As shown in Figure 8(a), the output power linearly increases with the pump power, with a slope efficiency of ∼83%. When the pump power reaches the maxima of 3573 W, the maximum output power reaches 3014 W. As shown in Figure 8(b), the spectra indicates that the Stokes light component intensity raises up to 54 dB when the output power reaches 3014 W, and the residual pump light intensity is 35 dB lower than the signal light. The time-domain signal detected by the photodetector and the corresponding FFT results at the output power of 3014 W are shown by the blue and red line in Figure 8(c). No obvious fluctuations are observed in time-domain traces, which indicate that the TMI threshold is higher than 3014 W under the condition of co-pump by 976 nm LDs. The measured result of M^2 factor and the beam profiles at different output power are shown in Figure 8(d). When the output power increases from 40 W to 3014 W, the M^2 factor increases from 1.34 to 1.37, the beam quality degradation is negligible.The experimental results show that the power scaling of this amplifier is limited by the available pump power, as well as SRS.

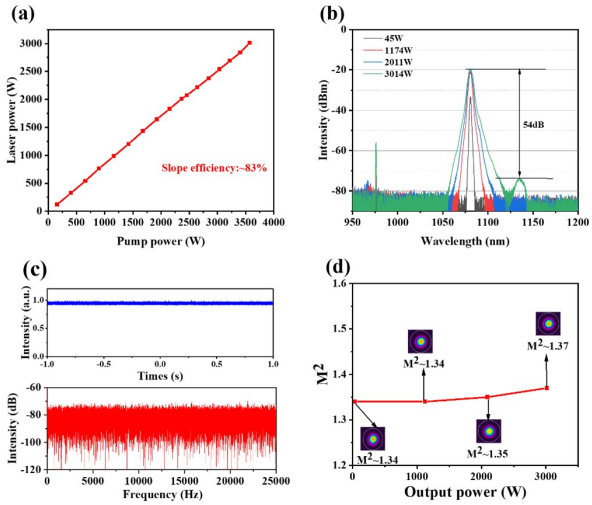

Figure 8. (a) Output power as a function of pump power in co-pump scheme; (b) Output spectra under different output power in co-pump scheme; (c) Time-domain signal and the corresponding FFT spectrum at 3014W; (d) M^2 factor as a function of output power in co-pump scheme. Insert: beam profiles at different output power.

Finally, the amplifier performance was investigated under the condition of bidirectional-pump at the same bending diameter. The experimental results are shown in Figure 9. In the bidirectional scheme, the co-pump power is increased to maxima of 3573 W first, and then the counter-pump power is subsequently increased, as shown in Figure 9(a). The output power increases approximately linearly with the pump power, with a slope efficiency of ∼81%. When the pump power is 8255 W, the maximum output power reaches 6740W. The slightly decreased slope efficiency could possibly result from the leaked HOMs power owing to degraded beam quality. As shown in Figure 9(b), the SRS suppression ratio is ∼30 dB under the output power of 6740 W. At the highest output power, no fluctuations appear in the time-domain signal, as well as its corresponding FFT spectra, as shown in Figure 9(c). The beam quality M^2 factor is measured and recorded during the experiment, the result and beam profiles are shown in Figure 9(d). At the highest output power, the M^2 factor is ∼1.49, maintaining a near-single-mode output. When the output power increases from 40 W to 6740 W, the M^2 factor increases from 1.37 to 1.49. These results indicate that the TMI threshold of this bidirectional-pump amplifier is higher than 6740 W. The output power and M^2 beam quality factor at the maximum output power exhibited stable performance over multiple consecutive measurements (spanning over six minutes). This

https://doi.org/10.1017/hpl.2025.10070 Published online by Cambridge University Press

consistent behavior demonstrates the system's operational stability and confirms the absence of TMI effects at the maximum output power. The output power can be further improved by increasing the co-pump power. However, in our case, the overall output power is constrained by the SRS, and further increasing the co-pump power would result in more severe nonlinear effects. Therefore, multiple measures, such as reducing the passive fiber length, should be taken concurrently to realize further power scaling.

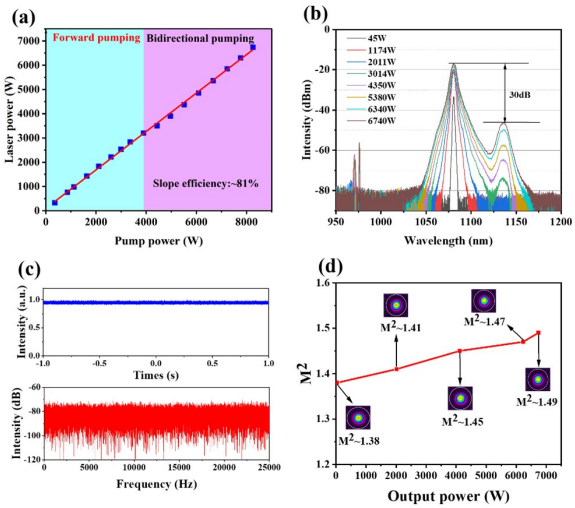

Figure 9. (a) Output power as a function of pump power in bidirectional-pump scheme; (b) output spectra under different output power in bidirectional-pump scheme; (c) time-domain signal and the corresponding FFT spectra at 6740W; (d) M^2 factor as a function of output power in bidirectional-pump scheme. Insert: beam profiles at different output power.

5. Conclusion

To summarize, we proposed a fiber design simultaneously integrating the optical confinement and gain tailoring design for TMI mitigation. The benefits of this fiber design are fully analyzed and recognized, according to which a low NA confined-doped fiber is developed. Consequently, by exploiting the self-developed low-NA confined-doped fiber, we obtained a 6.74 kW near-single-mode output laser, with a slope efficiency of ∼81%. At the maximum output power, the SRS suppression ratio is ∼30 dB, and the beam quality M^2 factor is ∼1.49. The further power scaling is limited by SRS. To our knowledge, this is the highest output power in a fiber laser employing the confined-doped or low NA fiber design that delivering near-single-mode beam quality (M^2<1.5). Further power scaling can be achieved by collaboratively optimizing the doping ratio, dopant distribution uniformity, core NA and the refractive index profile. We believe this work could provide a practical and effective approach for achieving higher output power with near-single-mode beam quality in large mode area fiber laser systems, and the fabrication simplicity would facilitate scalable deployment in high brightness laser applications.

Acknowledgement

This work was supported by the National Key Research and Development Program of China (2022YFB3606000), in part by the National Natural Science Foundation of China (62305390,62205373), in part by the Distinguished Young Scholars of Hunan Province (No.2023JJ10057). The authors would like to thank Yangying Zhou and Kun Zhang for their kind help during the experiment.

References

1. D. J. Richardson, J. Nilsson, and W. A. Clarkson, "High power fiber lasers: current status and future perspectives," *J. Opt. Soc. Am. B*, vol. 27, pp. B63–B92, Mar. 2010. DOI: 10.1364/JOSAB.27.000B63.
2. J. Hecht, "High-power fiber lasers," *Opt. Photon. News*, vol. 29, no. 10, pp. 30–37, Oct. 2018. DOI: 10.1364/OPN.29.10.000030.
3. W. Shi , Q. Fang, X. Zhu, R. A. Norwood, and N. Peyghambarian, "Fiber lasers and their applications [Invited]," *Appl. Opt.*, vol. 53, no. 28, pp. 6554–6568, Oct. 2014. DOI: 10.1364/AO.53.006554.
4. B. Shiner, "The Impact of Fiber Laser Technology on the World Wide Material Processing Market," in *CLEO: Applications and Technology*. OSA Technical Digest. USA, Jun. 2013, pp. AF2J.1. DOI: 10.1364/CLEO_AT.2013.AF2J.1.
5. L. Dong, J. Ballato, and J. Kolis, "Power scaling limits of diffraction-limited fiber amplifiers considering transverse mode instability," *Opt. Express*, vol. 31, no. 4, pp. 6690–6703, Feb. 2023. DOI: 10.1364/OE.483808.
6. M. N. Zervas, "Transverse mode instability, thermal lensing and power scaling in Yb^{3+}-doped high-power fiber amplifiers," *Opt. Express*, vol. 27, no. 13, pp. 19019–19041, Jun. 2019. DOI: 10.1364/OE.27.019019.
7. X. Chen , T. Yao, L. Huang, Y. An, H. Wu, Z. Pan, and P. Zhou, "Functional Fibers and Functional Fiber-Based Components for High-Power Lasers," *Adv. Fiber Mater.*, vol. 5, no. 1, pp. 59–106, Jan. 2023. DOI: 10.1007/s42765-022-00219-7.
8. V. Filippov, Y. Chamorovskii, J. Kerttula, K. Golant, M. Pessa, and O. G. Okhotnikov, "Double clad tapered fiber for high power applications," *Opt. Express*, vol. 16, no. 3, pp. 1929–1944, Feb. 2008. DOI: 10.1364/OE.16.001929.
9. X. Meng, Y. Ye, B. Yang, X. Xi, P. Wang, C. Shi, Z. Pan, L. Huang, H. Zhang, and X. Wang, "Demonstration of 3 kW-Level Nearly Single Mode Monolithic Fiber Amplifier Emitting at 1050 Nm Employing Tapered Yb-Doped Fiber," *IEEE Photon. J.*, vol. 15, no. 4, pp. 1–7, Aug. 2023. DOI: 10.1109/JPHOT.2023.3277201.
10. L. Zeng, X. Xi, Y. Ye, X. Lin, X. Wang, J. Li, C. Shi, B. Yang, H. Zhang, P. Wang, P. Zhou, and X. Xu , "A novel fiber laser oscillator employing saddle-shaped

https://doi.org/10.1017/hpl.2025.10070 Published online by Cambridge University Press

core ytterbium-doped fiber," *Appl. Phys. B*, vol. 126, no. 11, pp. 1–13, Nov. 2020. DOI: 10.1007/s00340-020-07533-1.

11. Y. Chen, Y. Ye, L. Huang, H. Yang, H. Wu, Z. Yan, Z. Pan, X Wang, Z. Wang, and P. Zhou, "5 kW-level single-mode fiber amplifier based on low-numerical-aperture fiber," *Chin. Opt. Lett.*, vol. 22, no. 4, pp. 76–81, Apr. 2024. DOI: 10.3788/COL202422.041404.
12. D. Jain, Y. Jung, P. Barua, S. Alam, and J. K. Sahu, "Demonstration of ultra-low NA rare-earth doped step index fiber for applications in high power fiber lasers," *Opt. Express*, vol. 23, no. 6, pp. 7407–7415, Mar. 2015. DOI: 10.1364/OE.23.007407.
13. F. Beier, C. Hupel, J. Nold, S. Kuhn, S. Hein, J. Ihring, B. Sattler, N. Haarlammert, T. Schreiber, R. Eberhardt, and A. Tünnermann, "Narrow linewidth, single mode 3 kW average power from a directly diode pumped ytterbium-doped low NA fiber amplifier," *Opt. Express*, vol. 24, no. 6, pp. 6011–6020, Mar. 2016. DOI: 10.1364/OE.24.006011.
14. F. Stutzki, F. Jansen, T. Eidam, A. Steinmetz, C. Jauregui, J. Limpert, and A. Tünnermann, "High average power large-pitch fiber amplifier with robust single-mode operation," *Opt. Lett.*, vol. 36, no. 5, pp. 689–691, Mar. 2011. DOI: 10.1364/OL.36.000689.
15. R. Dauliat, A. Benoît, D. Darwich, R. Jamier, J. Kobelke, S. Grimm, K. Schuster, and P. Roy, "Demonstration of a homogeneous Yb-doped core fully aperiodic large-pitch fiber laser," *Appl. Opt.*, vol. 55, no. 23, pp. 6229–6235, Aug. 2016. DOI: 10.1364/AO.55.006229.
16. R. du Jeu, R. Dauliat, B. Leconte, M. Malleville, R. Jamier, J. Bierlich, A. Schwuchow, K. Schuster, and P. Roy, "Polarization-maintaining Yb-doped large-mode-area fully aperiodic large-pitch fibers," *Appl. Opt.*, vol. 57, no. 29, pp. 8582–8585, Oct. 2018. DOI: 10.1364/AO.57.008582.
17. Y. Ying, X. Yan, D. Shan , Z. Gao, G. Si, G. Fu, and Q. Qi, "A review of recent research progress on optimization in D-shaped photonic crystal fiber," *Opt. Laser Technol.*, vol. 169, p. 110047, Jan. 2024. DOI: 10.1016/j.optlastec.2023.110047.
18. X. Chen, L. Huang, H. Yang, X. Xi, Y. An, Z. Yan, Y. Chen, Z. Pan, and P. Zhou, "Large-mode-area multi-resonant all-solid photonic bandgap fiber with low bending loss and robust single-mode operation," *Opt. Laser Technol.*, vol. 157, p. 108668, Jul. 2022. DOI: 10.1016/j.optlastec.2022.108668.
19. L. Dong, F. Kong, G. Gu, T. Hawkins, M. Jones, and J. Parsons, "Large-Mode-Area All-Solid Photonic Bandgap Fibers for the Mitigation of Optical Nonlinearities," *IEEE J. Sel. Top. Quantum Electron.*, vol. 22, no. 2, pp. 316–322, Mar. 2016. DOI: 10.1109/JSTQE.2015.2451012.
20. H. Wu, H. Li, Y. An, R. Li, X. Chen, H. Xiao, L. Huang, H. Yang, Z. Yan, J. Leng, Z. Pan, and P. Zhou, "Transverse mode instability mitigation in a high-power confined-doped fiber amplifier with good beam quality through seed laser control," *High Power Laser Sci. Eng.*, vol. 10, no. 06, pp. e44–e97, Dec. 2022. DOI: 10.1017/hpl.2022.31.
21. H. Wu, R. Li, H. Xiao, L. Huang, H. Yang, Z. Pan, J. Leng, and P. Zhou, "High-power tandem-pumped fiber amplifier with beam quality maintenance enabled by the confined-doped fiber," *Opt. Express*, vol. 29, no. 20, pp. 31337–31347, Oct. 2021. DOI: 10.1364/oe.435829.
22. L. Huang, H. Wu, R. Li, H. Xiao, H. Yang, Z. Yan, J. Leng, Z. Pan, and P. Zhou, "Homemade confined-doped fiber for 10 kW level fiber laser output with good beam quality," *High Power Laser Part. Beams*, vol. 34, no. 11, p. 111002, Nov. 2023. DOI: 10.11884/HPLPB202234.220232.
23. Y. Mashiko, H. K. Nguyen, M. Kashiwagi, T. Kitabayashi, K. Shima, and D. Tanaka, "2 kW single-mode fiber laser with 20-m long delivery fiber and high SRS suppression," in *Proc. SPIE*, San Francisco, CA, USA, Feb. 2016, Art. no. 972805. DOI: 10.1117/12.2212049.
24. S. Ikoma, H. K. Nguyen, M. Kashiwagi, K. Uchiyama, K. Shima, and D. Tanaka, "3 kW single-stage all-fiber Yb-doped single-mode fiber laser for processing of highly reflective and thermally conductive materials," in *Proc. SPIE*, San Francisco, CA, USA, Jan. 2017, Art. no. 100830Y. DOI: 10.1117/12.2250294.
25. C. P. Seah, W. Y. W. Lim, and S. L. Chua, "A 4 kW fiber amplifier with good beam quality employing confined-doped gain fiber," in *Proc. Laser Congr.*, Boston, MA, USA, Oct. 2018, Art. no. ATh4A.3. DOI: 10.1364/ASSL.2018.AM2A.2.
26. S. Chowdhury, D. Majumder, V. A. Gomes, D. Pal, A. Dhar, A. Pal, and D. Ghosh, "Beam quality evolution in large-mode-area specially doped laser fiber through bend-induced effective refractive index change," *Laser Phys.*, vol. 34, no. 4, p. 045104, Apr. 2024. DOI: 10.1088/1555-6611/ad2bec.
27. N. Choudhury, S. Chowdhury, S. D. Chowdhury, N. K. Shekhar, D. Jain, R. Sen, and A. Dhar "Novel dopant-tailored fibers using vapor-phase chelate delivery technique," *Phys. Status Solidi A*, vol. 219, no. 1, p. 2100484, Jan. 2022. DOI: 10.1002/pssa.202100484.
28. L. Liao, F. Zhang, X. He, Y. Chen, Y. Wang, H. Li, J. Peng, L. Yang, N. Dai, and J. Li, "Confined-doped fiber for effective mode control fabricated by MCVD process," *Appl. Opt.*, vol. 57, no. 12, pp. 3244–3249, Jun. 2018. DOI: 10.1364/AO.57.003244.
29. C. Ye, J. Koponen, T. Kokki, J. Montiel i Ponsoda, A. Tervonen, and S. Honkanen, "Near-diffraction-limited output from confined-doped ytterbium fibre with 41 μm

https://doi.org/10.1017/hpl.2025.10070 Published online by Cambridge University Press

core diameter," *Electron. Lett.*, vol. 47, no. 14, pp. 819–821, Jul. 2011. DOI: 10.1049/el.2011.1105.

30. J. R. Marciante, "Gain Filtering for Single-Spatial-Mode Operation of Large-Mode-Area Fiber Amplifiers," *IEEE J. Sel. Topics Quantum Electron.*, vol. 15, no. 1, pp. 30–36, Jan. 2009. DOI: 10.1109/JSTQE.2008.2010272.
31. Z. Zhang, X. Lin, X. Zhang, Y. Luo, S. Liao, X. Wang, G. Chen, Y. Xing, H. Li, J. Peng, N. Dai, J. Zhou, and J. Li, "Low-numerical aperture confined-doped long-tapered Yb-doped silica fiber for a single-mode high-power fiber amplifier," *Opt. Express*, vol. 30, no. 18, pp. 32333–32346, Sep. 2022. DOI: 10.1364/OE.466111.
32. H. Wu, R. Li, H. Xiao, L. Huang, H. Yang, J. Leng, Z. Pan, and P. Zhou, "First Demonstration of a Bidirectional Tandem-Pumped High-Brightness 8 kW Level Confined-Doped Fiber Amplifier," *J. Lightw. Technol.*, vol. 40, no. 16, pp. 5673–5681, Aug. 2022. DOI: 10.1109/JLT.2022.3183381.

https://doi.org/10.1017/hpl.2025.10070 Published online by Cambridge University Press